REPORTS

GEOPHYSICS

Local near instantaneously dynamically triggered aftershocks of large earthquakes

Wenyuan Fan* and Peter M. Shearer

Aftershocks are often triggered by static- and/or dynamic-stress changes caused by mainshocks. The relative importance of the two triggering mechanisms is controversial at near-to-intermediate distances. We detected and located 48 previously unidentified large early aftershocks triggered by earthquakes with magnitudes between ≥7 and 8 within a few fault lengths (approximately 300 kilometers), during times that high-amplitude surface waves arrive from the mainshock (less than 200 seconds). The observations indicate that near-to-intermediate-field dynamic triggering commonly exists and fundamentally promotes aftershock occurrence. The mainshocks and their nearby early aftershocks are located at major subduction zones and continental boundaries, and mainshocks with all types of faulting-mechanisms (normal, reverse, and strike-slip) can trigger early aftershocks.

Earthquake occurrence is modulated by complex fault interactions that often involve static- or dynamic-stress triggering mechanisms (*1*), which can trigger earthquakes over a variety of spatial and temporal scales (*2*–*4*). Aftershock sequences are thought to result from either or both of these mechanisms (*1*, *5*). Static-stress triggering is most important for near-field aftershocks, whereas dynamic triggering is dominant in the far field. However, it is challenging to quantitatively separate the effects of static and dynamic triggering in the near-to-intermediate field (*6*, *7*), leaving their relative importance controversial (*8*, *9*).

Dynamic triggering is most clearly seen at large distances from earthquakes, where earthquakes and/or nonvolcanic tremors sometimes occur during the passage of surface waves, which are generally the highest-amplitude wave arrivals from shallow sources (*10*–*12*). However, observing possible dynamic triggering close to earthquakes is hampered by the mainshock coda, leaving existing catalogs incomplete and the local dynamic triggering effects uncertain (*13*–*15*). More complete catalogs would help in understanding local tectonics, constraining fault strength, and forecasting potential host faults for large earthquakes (*16*). Local dynamic triggering can facilitate multiple-fault ruptures for a single earthquake, which can pose a much higher seismic risk than that of single-fault ruptures (*17*, *18*). Recently, local near-instantaneous dynamic triggering has been observed at both subduction zones (*19*) and continental plate boundaries (*20*, *21*). But it is unclear how commonly this type of triggering occurs. We performed a comprehensive global search for early aftershocks of 7 ≤ magnitude (M) < 8 earthquakes and found that local near-instantaneous dynamic triggering is common and that multiple-fault systems often dynamically interact with each other within a few fault lengths of the mainshocks within the first ~200 s.

We analyzed teleseismic P waves from 88 large earthquakes [7.0 ≤ moment magnitude (M_w) < 8.0] from January 2004 to September 2015, with Global Centroid Moment Tensor (GCMT) centroid depths shallower than 40 km (Fig. 1) (*22*). We did not examine 12 larger earthquakes (M_w ≥ 8.0) in the same period because of their duration and complexity. We applied back-projection to detect and locate early aftershocks. Back-projection has proven to be effective to resolve complex spatiotemporal evolution of large earthquakes because the method requires few prior assumptions (*23*), and it has been successfully implemented to detect and locate both subevents (*24*–*27*) and early aftershocks (*19*–*21*, *28*, *29*).

Our data are from global stations distributed by the Data Management Center (DMC) of the Incorporated Research Institutions for Seismology (IRIS). The P waves are filtered between 0.05 and 0.5 Hz for back-projection and are aligned for each event so as to reduce the effect of three-dimensional velocity structure (*30*). No post-smoothing or post-processing was applied to the back-projection images. We searched with a three-step screening criteria for potential early aftershocks that occurred within 200 s and between 50 and ~300 km from the target earthquakes (*30*). We have validated our detection algorithm with three tests (*30*), which include confirming that our detected early aftershocks can be seen in high-frequency regional array data (fig. S7), detecting and locating five cataloged mainshock–early-aftershock pairs within 100 km (fig. S8), and performing back-projection on 15 local M_w 5.5 to 6.5 earthquakes located 200 to 400 km away from mainshocks, using the same corrections as we used on the mainshocks (figs. S9 and S10).

Twenty-seven of the 88 target earthquakes clearly triggered early aftershocks and include events at most of Earth's subduction zones and continental boundaries (Fig. 1 and figs. S1 to S3). None of the 88 target earthquakes have cataloged aftershocks in the time/distance window that we examined for this study (*31*). Earthquakes with all types of faulting mechanisms are capable of triggering early aftershocks (16 reverse-faulting, 4 strike-slip, and 7 normal-faulting) (Figs. 1 and 2 and table S1). Normal-faulting earthquakes have the highest triggering rate (50%), whereas triggering rates of reverse-faulting (28.1%) and strike-slip (23.5%) earthquakes are similar. For robustness, our back-projection approach focuses on the phase of the P wave arrivals, at the cost of losing absolute P wave amplitudes (*30*), which makes estimating the magnitudes of the very early aftershocks challenging. Nevertheless, by comparing with historical nearby earthquakes, the triggered early aftershocks are likely to be M 5 to 6.5 earthquakes (*30*).

Within the Sunda arc subduction zone, a 24 July 2005 earthquake (M_w 7.2) occurred near the northwestern boundary of the great 2004 Sumatra-Andaman earthquake (Fig. 2A) (*23*). The earthquake was a strike-slip event, which likely ruptured a different fault than the megathrust. The earthquake triggered two early aftershocks ~177 and ~221 km away from the epicenter and ~68 and 120 s after its initiation at the landward region of the subduction zone. The triggered events strongly correlate with the surface-wave arrivals from the mainshock. The exact focal mechanisms, magnitudes, and depths of the triggered events are difficult to determine with only teleseismic P waves (*19*), but the triggered events must be at least M 5 to be observed in the far field (*19*). Within 100 km of the 24 July 2005 earthquake, a 26 December 2004 reverse-faulting earthquake (M_w 7.2) triggered an event in the seaward region (fig. S1E). Both M 7 earthquakes may be aftershocks of the 2004 Sumatra-Andaman earthquake yet have very different focal mechanisms. Their triggered events are located in both the seaward and landward regions of the trench, indicating that the region is potentially critically stressed at both sides of the trench.

Within the Japan subduction zone, a 25 October 2013 normal-faulting earthquake (M_w 7.1) broke the shallow part of the Pacific plate mantle 2 years after the 2011 Tohoku earthquake (Fig. 2B). The earthquake is seaward of the trench and triggered an early aftershock landward of the trench axis ~40 s later. The triggered event is ~133 km away from the epicenter, close to the 2011 Tohoku earthquake centroid location, and can be either an interplate or intraplate earthquake (*32*). This triggered event underlines that stress

Scripps Institution of Oceanography, University of California, San Diego, La Jolla, CA 92093-0225, USA.
*Corresponding author. Email: w3fan@ucsd.edu

can be near instantaneously dynamically transferred within complex multiple fault systems, in a region with long-term plate-bending and converging deformation.

At the New Britain trench, the 29 March 2015 and 5 May 2015 M_w 7.5 doublet occurred on or near the subduction interface 130 km away from Kokopo, Papua New Guinea (Fig. 2C). The doublet events share similar focal mechanisms (*22*), and the 5 May 2015 event triggered two early aftershocks within the first 2 min after its initiation. The rupture propagated northeastward, toward the two triggered events (Fig. 2C). The first early aftershock is triggered ~40 s after the mainshock origin time, located ~120 km northeast of the mainshock epicenter, and is close to the 29 March 2015 M_w 7.5 earthquake epicenter. Even though the first early aftershock struck within the trench-parallel region, its clear spatiotemporal separation from the mainshock and spatial correlation with the 29 March 2015 earthquake suggest that it is an early aftershock rather than part of the mainshock. The second triggered early aftershock is located further north of the mainshock, which we refer to as the horizontal down-dip direction of the mainshock. The second triggered event is located by the Manus trench, where the Australian and Pacific plates converge at more than 70 mm year^{-1} (*33*). The convergence dominates the local tectonic evolution (*34*), and the triggered early aftershock implies that the interplate fault of the two plates might be critically stressed.

In total, the 27 large earthquakes triggered 48 early aftershocks with epicentral distances ranging from 54 to 334 km (Fig. 3). For each triggered event, the triggering time is taken as the delay from the origin time to the peak amplitude time within a 20-s stacking window at the triggered location, ranging from 29.7 to 193.3 s, from which a triggering velocity can be derived from the epicentral distance divided by

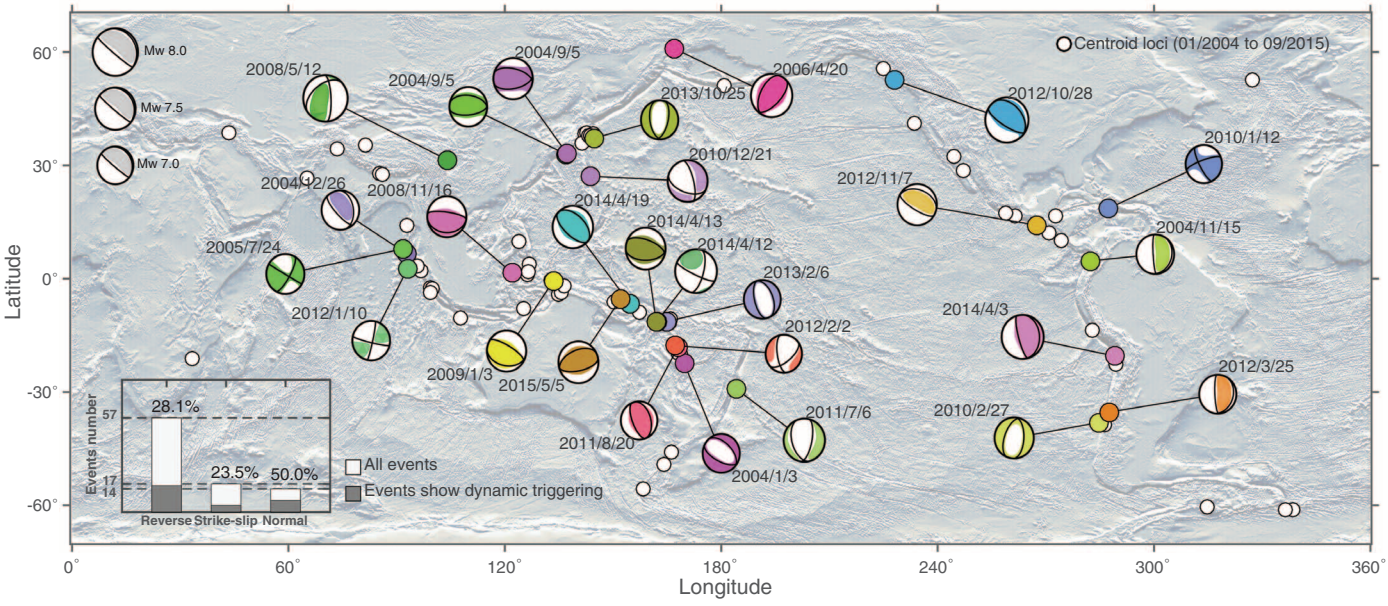

Fig. 1. Twenty-seven early-aftershock–triggering mainshocks and their focal mechanisms. The 27 triggering mainshocks are color-coded at their GCMT centroid locations (colored circles). The white circles show the rest of the 88 large earthquakes ($7 \le M_w < 8$) that we investigated with back-projection. Strike-slip earthquakes are defined when the rakes of both nodal planes are within 45° deviation of 0° or 180°. Normal- and reverse-faulting earthquakes have rakes within 45° deviation of −90° and 90°, respectively. (**Inset**) Triggering rates for the three types of earthquakes.

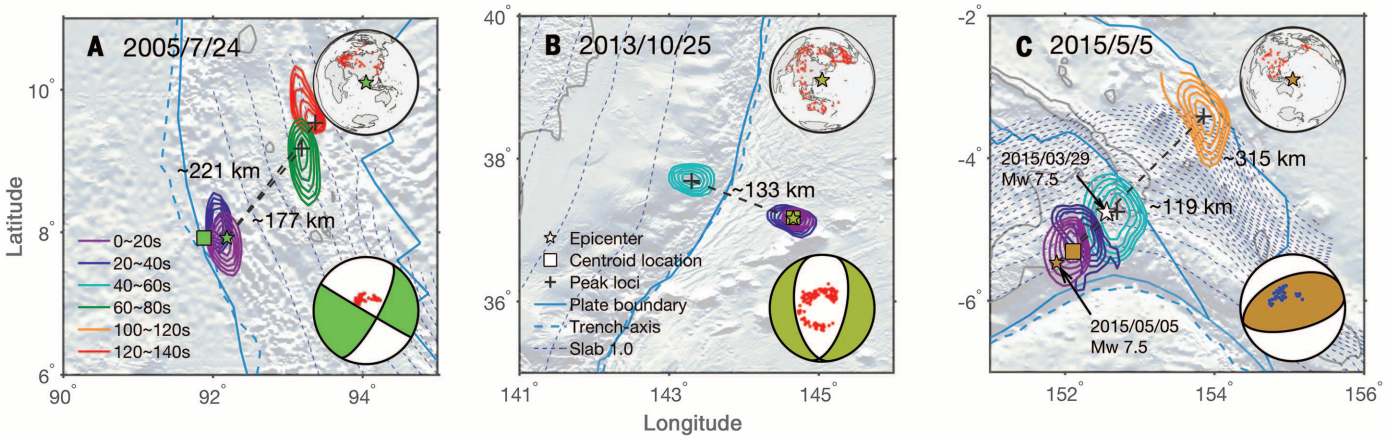

Fig. 2. Back-projection results for three earthquakes with different focal mechanisms (60% normalized energy contours). (**A**) Rupture evolution of the 24 July 2005, M_w 7.2 strike-slip earthquake in the Sunda arc. Stations used for back-projection and their *P* wave polarity with the GCMT focal mechanism are shown as insets. Negative polarities are red, and positive polarities are blue. (**B**) Rupture evolution of the 25 October 2013, M_w 7.1 normal-faulting earthquake in the Japan subduction zone. The insets are the same as in (A). (**C**) Rupture evolution of the 5 May 2015, M_w 7.5 reverse-faulting earthquake in the New Britain trench. The insets are the same as in (A).

the triggering time. To assess standard errors (SEs) in the epicentral distances and triggering times, we implemented jackknife resampling for each earthquake with the records used for the back-projection (*30*). Within 1 SE, all the triggered early aftershocks occurred after the surface wave passed through (at 3 to ~4 km/s) (Fig. 3). This strong correlation shows that the 48 early aftershocks were triggered by the mainshocks and suggests that dynamic stress was the physical process that drove the observed triggering. Assuming that the *M* 7 earthquakes ruptured for ~40 s, then 26 triggered early aftershocks coincide with the passing surface waves (Fig. 3). The rapid-onset dynamic triggering events with small delay time indicate frictional failures caused by dynamic stress changes induced by the transient surface waves (*10*). In addition, 22 triggered events are delayed for seconds to minutes, which might reflect nonlinear friction behavior or a hydraulic response of the receiver faults (*35*–*37*). The diversity of the triggered responses suggests the heterogeneity of the stress field and the variability of the frictional strength at each given fault (*38*). These observations imply that dynamic triggering modulates near-to-intermediate field seismicity and commonly promotes large early aftershocks in a near-instantaneous fashion.

There are 11 triggered early aftershocks that occurred within 50 s of the origin time, with the remainder occurring within 200 s. The short temporal delay has two implications. First, a large portion of the early aftershocks are missing from global catalogs, which do not have these events, despite being large enough to be detected in teleseismic records. Second, the transition time from mainshock to aftershocks is near instantaneous at most of the subduction zones and plate boundaries via dynamic triggering. If the early aftershock sequence follows Omori's law, then the relative aftershock deficit, related to parameter *c*, will be pushed to as short as tens of seconds (*30*). If the aftershock activities are dominated by rate-and-state friction, then the derived *c* can be used to probe frictional properties of the local fault systems (*39*).

Most of the observed early aftershocks are unlikely to be on or near the mainshock slip surface. The early aftershocks have a distinctly different epicentral distance distribution than the aftershocks cataloged by the International Seismological Centre (ISC) (*31*) catalog or U.S. Geological Survey National Earthquake Information Center Preliminary Determination of Epicenters Bulletin (PDE) (Fig. 4A). The aftershock distribution of the ISC and PDE events can be used to estimate mainshock rupture areas. The majority of the catalog aftershocks are within ~90 km, whereas the majority of the dynamically triggered early aftershocks are more than ~90 km away from the epicenters (Fig. 4A) (*30*).

Fifteen of the 27 large earthquakes were reverse-faulting earthquakes at subduction zones, seven were normal-faulting earthquakes at subduction zones, four were strike-slip, and one was the 2008 China Wenchuan continental earthquake (reverse-faulting). All the subduction zone

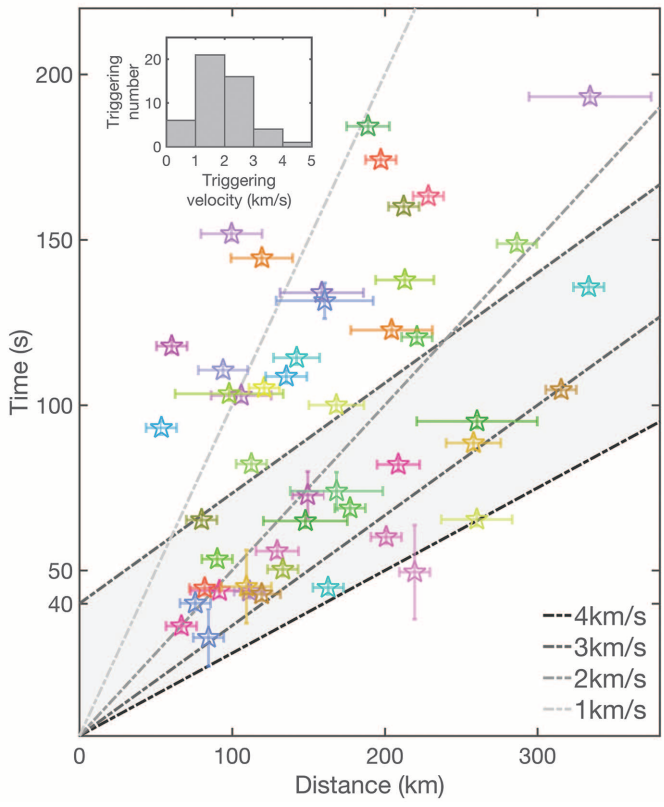

Fig. 3. Time versus distance plot of triggered events. Forty-eight triggered early aftershocks are shown as stars with the same color of their triggering large earthquakes. The colored bars for each triggered early aftershock show 1 SE of the epicentral distances and triggering times (table S1). The shaded region shows the likely influence of passing surface waves of a ~40 s duration *M* 7 earthquake. (Inset) The distribution of the triggering velocity for the 48 triggered events.

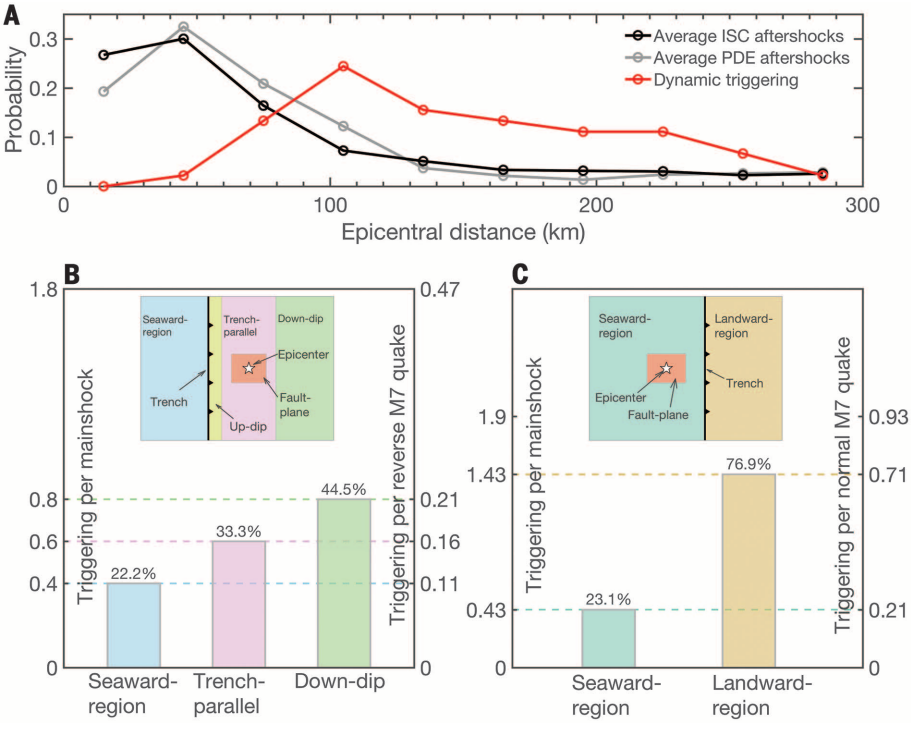

Fig. 4. Aftershock distribution and relative locations of the triggered early aftershocks. (**A**) The averaged ISC aftershock distribution of 18 mainshocks (*30*) is shown as the black line. Average PDE aftershock distribution from five mainshocks is shown as the gray line. The dynamically triggered early aftershock distribution is shown as the red line. The distribution is obtained from partitioning the triggered early aftershocks into 30-km-wide bins in epicentral distance. The probabilities are placed in the middle of the center of each epicentral bin. (**B**) Triggering rate and distribution for reverse-faulting mainshocks. (**C**) Triggering rate and distribution for normal-faulting mainshocks. (Insets) The divisions of the relative locations of triggered early aftershocks.

reverse-faulting earthquake centroid locations were within the landward region, whereas all the normal-faulting earthquakes were in the seaward region of the subduction zone (figs. S1 to S3). To better understand the triggering mechanisms, we horizontally divided the triggered locations as down-dip region, trench-parallel region, up-dip region, and seaward region for reverse-faulting earthquakes with respect to the mainshock and trench axis; we divided the triggered locations as landward and seaward regions for normal-faulting earthquakes with respect to the trench axis (Fig. 4, B and C). For the reverse-faulting earthquakes, the dynamically triggered early aftershocks tend to occur in the down-dip region (44.5%), rather than the trench-parallel region (33.3%) or the seaward region (22.2%). We did not observe any triggered early aftershocks in the up-dip region for reverse-faulting earthquakes. For the normal-faulting earthquakes, occurrence of the triggered early aftershocks in the landward region is three times higher than in the seaward region (landward region, 76.9%; seaward region, 23.1%). In total, the faults in the landward region, either on or near the megathrust, are more susceptive to near-field dynamic triggering. Although tsunami earthquakes often rupture the shallowest portion of the megathrust (*40*), the material or the faults in that region may be too weak to accumulate enough strain to be dynamically triggered. Generally, extensional regions are more easily triggered than compressional regions (*41*, *42*). If this holds true, some of the triggered earthquakes in the landward region are likely normal-faulting instead of reverse-faulting.

The detected early aftershocks all radiated less energy than that of the mainshocks and are likely moderate in size (M 5 to 6.5) (*30*). Although observed remotely triggered earthquakes to date have been relatively small (*43*), it is possible on rare occasions that remote dynamic triggering could cause damaging earthquakes (*44*). Near-to-intermediate field triggering has been observed before (*24*–*27*, *45*–*48*)—and occurs in physics-based rupture models that show that multiple-fault systems can rupture together in a single earthquake (*17*, *18*, *49*–*51*)—but is often considered to be part of the mainshock rupture process, which may involve multiple subevents, some triggered in response to both static- and dynamic-stress changes. Because the majority of the triggered early aftershocks are seen in the landward region of the trenches (Fig. 4), which could be on or near the megathrust, it is possible that this type of early dynamic triggering could lead to a great earthquake ($M \geq 8.0$), with contributions from both static and dynamic triggering (*49*, *51*, *52*). However, in the absence of known fault geometries for the triggered earthquakes we observed, it is difficult to perform stress calculations in order to explore the triggering mechanisms in more detail.

Early dynamically triggered aftershocks can also be seen in standard earthquake catalogs in favorable circumstances. To compare with our back-projection-detected events, we systematically searched through the ISC catalog from 1993 to 2013 to find earthquakes occurring in the same space/time window that we searched using back-projection, which follow target events of varying sizes (*30*). The local near-instantaneous triggering rate drawn from the ISC catalog for M 7 earthquakes (4 of 198) is much lower than what we observed with back-projection (27 of 88), highlighting the difficulty in detecting these early aftershocks with standard methods (fig. S11). The catalog results are most likely to be complete in cases in which the triggered event is larger than the target event—the target event is a foreshock to the later event. This occurs globally in our space/time window for 3 of 1532 (0.2%) of $M >$ 6 earthquakes. Assuming that the dynamically triggered earthquake magnitudes are drawn randomly from a b = 1 Gutenberg-Richter distribution and that aftershock triggering rates are self-similar with magnitude (*53*), a 0.2% rate of triggering a larger event implies a 20% rate of M 5 to 7 early aftershocks following M 7 mainshocks in the same space/time window. This is comparable with our observed rate of 30%.

Our analysis represents a lower limit on the number of near-source dynamically triggered earthquakes that are large enough to be seen teleseismically because we likely missed many events owing to our conservative selection criteria and the poor station coverage for some mainshocks. Thus, fault interactions and triggering may be a relatively common feature for large earthquakes near subduction zones and continental boundaries. The near-zero to short delay time of the observed dynamic triggering suggests that in a large complex fault system, such as exists in most subduction zones, a few faults will always be critically stressed and close to failure. By studying where triggered events are most common, it may be possible to infer properties of the interacting faults in specific regions. Last, early aftershocks can potentially illuminate unknown faults, and the observed fault interactions of earthquake sequences can inform future hazard assessment.

REFERENCES AND NOTES

1. R. A. Harris, *J. Geophys. Res.* **103**, 24347–24358 (1998).
2. D. P. Hill *et al.*, *Science* **260**, 1617–1623 (1993).
3. G. C. P. King, R. S. Stein, J. Lin, *Bull. Seismol. Soc. Am.* **84**, 935–953 (1994).
4. J. Gomberg, P. A. Reasenberg, P. Bodin, R. A. Harris, *Nature* **411**, 462–466 (2001).
5. A. M. Freed, *Annu. Rev. Earth Planet. Sci.* **33**, 335–367 (2005).
6. C. Voisin, M. Campillo, I. R. Ionescu, F. Cotton, O. Scotti, *J. Geophys. Res.* **105**, 21647–21659 (2000).
7. J. Decriem *et al.*, *Geophys. J. Int.* **181**, 1128–1146 (2010).
8. K. R. Felzer, E. E. Brodsky, *Nature* **441**, 735–738 (2006).
9. K. Richards-Dinger, R. S. Stein, S. Toda, *Nature* **467**, 583–586 (2010).
10. D. Kilb, J. Gomberg, P. Bodin, *Nature* **408**, 570–574 (2000).
11. K. Obara, *Science* **296**, 1679–1681 (2002).
12. A. A. Velasco, S. Hernandez, T. O. M. Parsons, K. Pankow, *Nat. Geosci.* **1**, 375–379 (2008).
13. Y. Y. Kagan, *Bull. Seismol. Soc. Am.* **94**, 1207–1228 (2004).
14. Z. Peng, J. E. Vidale, H. Houston, *Geophys. Res. Lett.* **33**, L17307 (2006).
15. Z. Peng, P. Zhao, *Nat. Geosci.* **2**, 877–881 (2009).
16. S. G. Wesnousky, *Bull. Seismol. Soc. Am.* **84**, 1940–1959 (1994).
17. R. A. Harris, R. J. Archuleta, S. M. Day, *Geophys. Res. Lett.* **18**, 893–896 (1991).
18. R. A. Harris, J. F. Dolan, R. Hartleb, S. M. Day, *Bull. Seismol. Soc. Am.* **92**, 245–255 (2002).
19. W. Fan, P. M. Shearer, *Geophys. Res. Lett.* **43**, 1934–1942 (2016).
20. E. Nissen *et al.*, *Nat. Geosci.* **9**, 330–336 (2016).
21. D. Wang *et al.*, *J. Geophys. Res.* **121**, 1948–1961 (2016).
22. G. Ekström, M. Nettles, A. Dziewoński, *Phys. Earth Planet. Inter.* **200-201**, 1–9 (2012).
23. M. Ishii, P. M. Shearer, H. Houston, J. E. Vidale, *Nature* **435**, 933–936 (2005).
24. B. P. Allmann, P. M. Shearer, *Science* **318**, 1279–1283 (2007).
25. E. Kiser, M. Ishii, *Geophys. Res. Lett.* **38**, L07301 (2011).
26. H. Yue, T. Lay, K. D. Koper, *Nature* **490**, 245–249 (2012).
27. L. Meng, J.-P. Ampuero, A. Sladen, H. Rendon, *J. Geophys. Res.* **117**, 2156–2202 (2012).
28. S. D'Amico, K. D. Koper, R. B. Herrmann, A. Akinci, L. Malagnini, *Geophys. Res. Lett.* **37**, L03301 (2010).
29. E. Kiser, M. Ishii, *J. Geophys. Res.* **118**, 5564–5576 (2013).
30. Materials and methods are available as supplementary materials on *Science* Online.
31. International Seismological Centre, *On-line Bulletin* (ISC, 2013).
32. W. Nakamura, N. Uchida, T. Matsuzawa, *J. Geophys. Res.* **121**, 2591–2607 (2016).
33. C. DeMets, R. G. Gordon, D. F. Argus, S. Stein, *Geophys. Res. Lett.* **21**, 2191–2194 (1994).
34. T. Johnson, P. Molnar, *J. Geophys. Res.* **77**, 5000–5032 (1972).
35. J. Gomberg, M. L. Blanpied, N. M. Beeler, *Bull. Seismol. Soc. Am.* **87**, 294–309 (1997).
36. T. Parsons, *Geophys. Res. Lett.* **32**, L04302 (2005).
37. A. Nur, J. R. Booker, *Science* **175**, 885–887 (1972).
38. L. Rivera, H. Kanamori, *Geophys. Res. Lett.* **29**, 12-1 (2002).
39. Z. Peng, J. E. Vidale, M. Ishii, A. Helmstetter, *J. Geophys. Res.* **112**, B03306 (2007).
40. H. Kanamori, *Phys. Earth Planet. Inter.* **6**, 346–359 (1972).
41. S. Prejean, D. Hill, Dynamic triggering of earthquakes, in *Encyclopedia of Complexity and Systems Science* (Springer, 2009), pp. 2600–2621.
42. R. M. Harrington, E. E. Brodsky, *Bull. Seismol. Soc. Am.* **96**, 871–878 (2006).
43. T. Parsons, J. O. Kaven, A. A. Velasco, H. Gonzalez-Huizar, *Geochem. Geophys. Geosyst.* **13**, Q06016 (2012).
44. F. F. Pollitz, R. S. Stein, V. Sevilgen, R. Bürgmann, *Nature* **490**, 250–253 (2012).
45. D. Eberhart-Phillips *et al.*, *Science* **300**, 1113–1118 (2003).
46. D. D. Oglesby, D. S. Dreger, R. A. Harris, N. Ratchkovski, R. Hansen, *Bull. Seismol. Soc. Am.* **94**, S214–S233 (2004).
47. B. Delouis, M. Pardo, D. Legrand, T. Monfret, *Bull. Seismol. Soc. Am.* **99**, 87–94 (2009).
48. S. Peyrat *et al.*, *Geophys. J. Int.* **182**, 1411–1430 (2010).
49. G. Anderson, B. Aagaard, K. Hudnut, *Science* **302**, 1946–1949 (2003).
50. D. D. Oglesby, *Bull. Seismol. Soc. Am.* **95**, 1604–1622 (2005).
51. J. C. Lozos, *Sci. Adv.* **2**, e1500621 (2016).
52. D. C. Agnew, L. M. Jones, *J. Geophys. Res.* **96**, 11959–11971 (1991).
53. K. R. Felzer, R. E. Abercrombie, G. Ekström, *Bull. Seismol. Soc. Am.* **94**, 88–98 (2004).

ACKNOWLEDGMENTS

The facilities of IRIS Data Services, and specifically the IRIS DMC, were used for access to waveforms used in this study (National Science Foundation grant EAR-1261681). Hi-net data were obtained from the National Research Institute for Earth Science Disaster Prevention in Japan (NIED). The earthquake catalogs were downloaded from the Global Centroid Moment Tensor project (GCMT) (*22*), U.S. Geological Survey National Earthquake Information Center PDE, and ISC (*31*). The data used in the study are publicly available at DMC and NIED, and the processed data are available from the authors upon request. This work was supported by National Science Foundation grant EAR-1111111.

SUPPLEMENTARY MATERIALS

www.sciencemag.org/content/353/6304/1133/suppl/DC1
Materials and Methods
Supplementary Text
Figs. S1 to S11
Table S1 to S3
References (*54*–*75*)

29 April 2016; accepted 11 August 2016
10.1126/science.aag0013

Local near instantaneously dynamically triggered aftershocks of large earthquakes

Wenyuan Fan and Peter M. Shearer

Science **353** (6304), 1133-1136.
DOI: 10.1126/science.aag0013